Preprint
UCRL-JC-151940

Dislocation-Defect Interactions in Materials

J.S. Robach, I.M. Robertson, D.C. Ahn, P. Sofronis, B.D. Wirth, T. Arsenlis

This article was submitted to
The Minerals, Metals and Materials Society 2003 Annual Meeting and Exhibition
San Diego, CA, March 2-6, 2003

February 27, 2003

U.S. Department of Energy

Lawrence
Livermore
National
Laboratory

Dislocation-defect interactions in materials

J. S. Robach[*], I. M. Robertson[*], D. C. Ahn[**], P. Sofronis[**], B. D. Wirth[†], and T. Arsenlis[†]

[*] *University of Illinois, Department of Materials Science and Engineering, Urbana, Illinois 61801, USA*
[**] *University of Illinois, Department of Theoretical and Applied Mechanics, Urbana, Illinois 61801, USA*
[†] *Lawrence Livermore National Laboratory, 7000 East Avenue, L-353, Livermore, California 94550, USA*

ABSTRACT

In order to develop predictive models of the mechanical response of irradiated materials it is necessary to understand the fundamental physical processes controlling the deformation. This is particularly important near yielding where local defect interactions may dominate the behaviour. Dislocation-defect interactions in copper containing various densities and distributions of stacking-fault tetrahedra and small dislocation loops were examined dynamically using the in-situ TEM straining technique. Defect annihilation mechanisms as well as the conditions required to produce defect-free channels are proposed. The experimental results are compared to atomistic simulations and continuum mechanics calculations of unit interactions. Based on these observations, an improved continuum model of the mechanical behaviour of irradiated materials is presented.

§1. INTRODUCTION

The interactions of irradiation-induced defects with dislocations in reactor materials can have large and detrimental effects on their mechanical properties. Generally, ductility is reduced while yield and tensile strength increase with dose. At higher doses, an upper yield point occurs followed by softening. Figure 1 shows these trends occur in HCP (Himbeault *et al.*, 1994), BCC (Muller *et al.*, 1994) and FCC (Victoria *et al.*, 2000) pure materials and alloys. These features are also observed in materials irradiated with neutrons, protons, heavy-ions and electrons, showing the effect is independent of the irradiating particle.

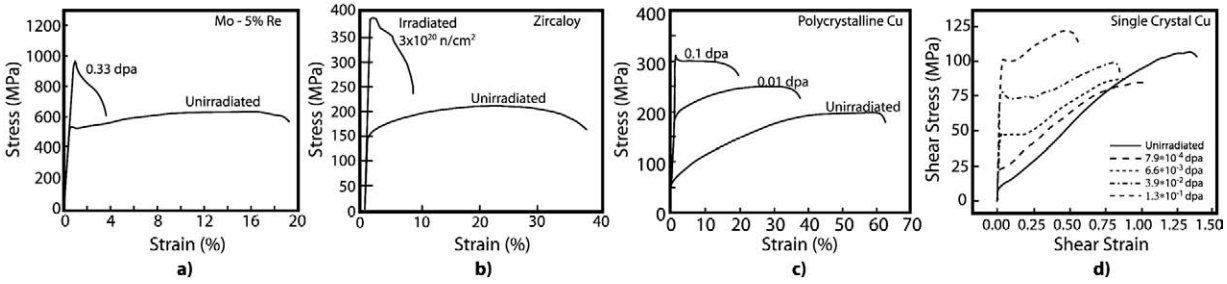

Figure 1. Comparison of the stress-strain curves for (a) proton-irradiated Mo-5% Re alloy (Muller *et al.*, 1994), (b) neutron-irradiated HCP Zircaloy (Meyers and Chawla, 1984), (c) neutron-irradiated polycrystalline copper (Singh *et al.*, 1995), and (d) proton-irradiated single crystal copper (Victoria *et al.*, 2000).

In the early stages of deformation of irradiated materials, mobile dislocations interact with and destroy the radiation-induced defects to create defect-free channels, as shown in figure 2. Creation of these channels requires the passage of numerous dislocations with the same Burgers vector on parallel slip planes. These channels form at low strains and subsequent plasticity is confined to them. Although *ex-situ* TEM studies have shown the existence of these channels in a range of irradiated materials the mechanism of channel initiation and extension as well as the detailed defect-annihilation dislocation reactions are not known (Okada *et al.*, 1989, Saka *et al.*, 1975). Many annihilation mechanisms have been proposed (Foreman and Sharp, 1969, Hirsch, 1976, Kimura and Maddin, 1965, Saada and Washburn, 1963), yet there is little supporting experimental evidence. In developing a physically based model capable of accounting for the yield strength increase as well as any subsequent softening, the mechanisms of channel initiation and defect annihilation must be incorporated.

Heavy-ion irradiation of copper produces mostly vacancy-type Frank loop defects (diameter=3 nm), with a minority of stacking fault tetrahedra (Kirk *et al.*, 2000, Stathopoulos, 1981). Electron irradiation and rapid quenching of low stacking fault energy metals can produce a high density of partially faulted Frank loops, or fully-formed stacking fault tetrahedra (Kojima *et al.*, 1989). In this paper, the interaction of glissile dislocations with both vacancy loops and

stacking fault tetrahedra in pure copper is presented along with molecular dynamics computer simulations and continuum calculations of similar interactions. The combination of the simulations and experimental results provides the basis of a new continuum model that predicts the important features of the mechanical behaviour of irradiated materials.

§2. EXPERIMENTAL PROCEDURE

Specimens of 99.999% pure polycrystalline Cu were cut from 250μm thick cold rolled strip into 11mm×2.7mm pieces. Holes were drilled in the ends of these pieces for attachment to the straining stage, and were mechanically polished to a 600-grit finish. The samples underwent an annealing treatment at 1023°K in a vacuum furnace for 2 hours and then were furnace-cooled to produce large equiaxed grains. Some of these annealed specimens were rapidly quenched from 980°C into iced brine at –10°C to produce stacking-fault tetrahedra throughout the specimens. The central sections of all specimens were thinned to electron transparency by jet-electropolishing in a solution of 33% nitric acid in methanol cooled to –20°C at a current density of 0.11A cm^{-2}.

Some of the electron transparent samples were irradiated with 200 keV Kr^{+} ions to a fluence between 1×10^{11} and 1×10^{13} ions cm^{-2} (approximately 2×10^{-4} to 2×10^{-2} dpa) at room temperature in the intermediate voltage transmission electron microscope at Argonne National Laboratory (Allen and Ryan, 1997). TRIM simulations show that the damage is created throughout the foil thickness (Ziegler, 1999). Straining of the rapidly quenched specimens and the irradiated specimens was performed in a JEOL 4000 EX TEM at the University of Illinois. The *in-situ* TEM straining experiments were recorded via a Gatan TV-rate camera onto S-VHS videotape for later analysis on a digital video editing system.

§3. EXPERIMENTAL RESULTS AND DISCUSSION

In the heavy-ion irradiated specimens, the defect density was homogeneous, with defects distributed throughout the foil. No defects decorated the pre-existing dislocations. The interstitials created by the irradiation are assumed lost to the foil surfaces. Vacancy-type loops and partially dissociated Frank loops were observed with a relatively low matrix dislocation density. During straining, some of the pre-existing dislocations moved and interacted with the irradiation-produced defects. These dislocations percolated small distances through the radiation-induced defect field, as shown in figure 2. The images in figure 2a-d are individual frames from videotape and illustrate the motion of a pre-existing dislocation through the defect field under an applied load. The extent of the dislocation motion is easier to visualize in figures 2e-h, which are composite images created by superimposing positive and negative frames. The unchanged regions in the composite images cancel, making the motion easily visible. Figure 2f illustrates the total movement observed during straining produced by the limited motion of small dislocation segments. This percolation was often observed alongside other sessile dislocations demonstrating that pre-existing dislocations do not contribute significantly to the total plasticity.

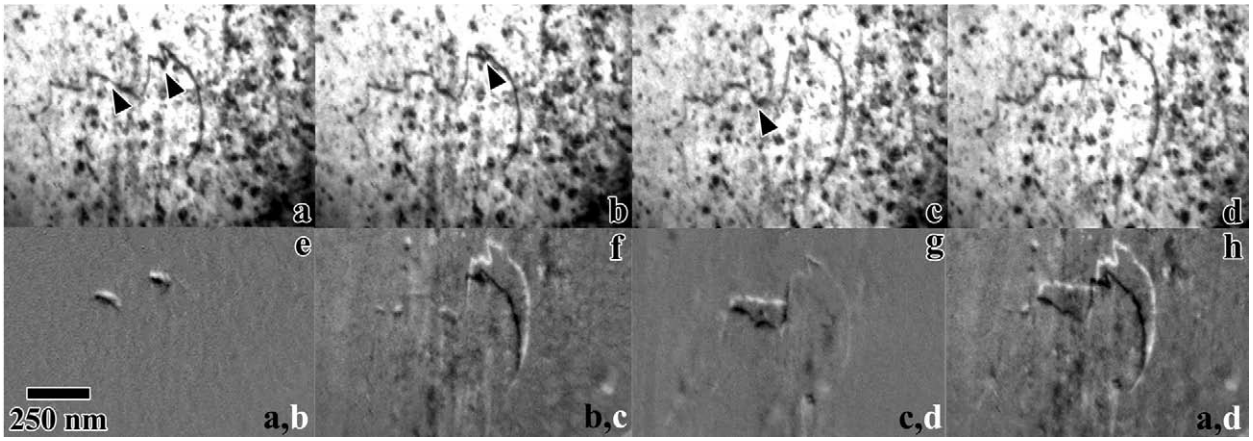

Figure 2. Bright field images showing the percolation of pre-existing dislocations through the defect field, (a)-(d). Comparison images with the white dislocation showing the dislocation position at the later time, (e)-(h). Arrows indicate pinned points about to break free in the next frame.

Dislocations responsible for creating the defect-free channels were observed to originate from grain boundaries and local stress concentrations (Robach *et al.*, 2003). This observation is contrary to the assumption made in many current models that pre-existing dislocations, once free from the stress field of a "defect cloud", act as sources on the interiors of grains, producing defect-free channels (Ghoniem *et al.*, 2001, Singh *et al.*, 1997, Sun *et al.*, 2000, Trinkaus *et al.*, 1997). The dynamic experiments revealed that grain boundaries and local stress concentrators act as dislocation sources. An example of this is shown in figure 3, in which the channels are seen extending from a crack flank. At some critical local shear stress, new dislocations are able to move out into the defect field within the grain. These dislocations eliminate defects and create an easy-slip channel for subsequent dislocations. These observations suggest the yield point phenomenon is a matter of dislocation propagation from active sources, not the sudden unlocking of sources from a "defect cloud".

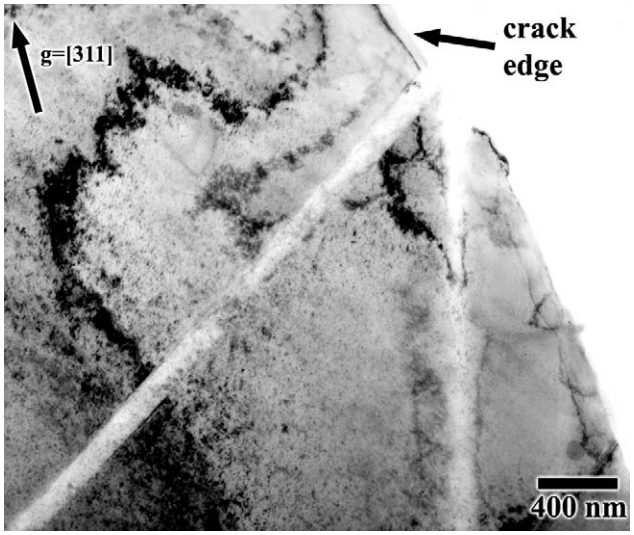

Figure 3. Well-developed defect-free channels originating from a crack tip. Here, the crack has already passed and the arrow indicates the crack face. The black dots are heavy-ion irradiation damage.

The defects were relatively strong obstacles to the motion of dislocations. The dynamic observations of the interactions reveal that a single interaction is not necessarily sufficient to annihilate a defect. The efficiency with which a dislocation annihilates a defect depends on the defect type and dislocation character. Screw dislocations are more effective than edge dislocations at removing defects (Robach *et al.*, 2003). These observations are also at variance with a basic premise of current models where it is assumed that a single interaction is sufficient for defect annihilation.

The direct observation of the dislocation-defect interaction permits the obstacle strength to be determined from the curvature of the dislocation in the video frame just prior to breakaway. The critical angle ($2\phi_c$) at breakaway is defined as the angle between tangents drawn from the intersection point of two circles that approximate the curvature between pinning points, as shown in figure 4. The local pinning point separation, l, is also measured from these captured video frames. These measured parameters are related to the athermal breakaway shear stress, τ_c, using the Fleischer-Friedel relationship (Fleischer, 1963, Friedel, 1964),

$$\tau_c = \frac{Gb}{l}(\cos\phi_c)^{\frac{3}{2}}. \quad (1)$$

Here, G is the shear modulus (55 GPa for Cu) and b is the magnitude of the Burgers vector of the dislocation (b_{Cu} = 0.255nm). This equation is based on a statistical analysis of how many defects a dislocation will encounter as it sweeps out an arc between pinning points within its slip plane.

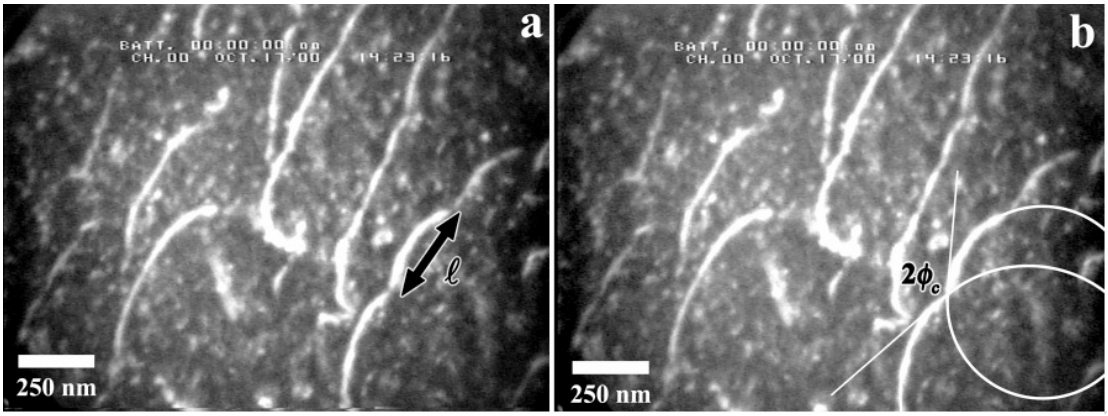

Figure 4. The distance between pinned segments, *l*, is measured from a captured frame, (a). The method for measuring the critical bowing angle prior to breakaway is shown in (b).

A histogram of the local critical stresses calculated for fifty-one dislocation-defect interactions for copper irradiated to a fluence of 5×10^{12} Kr^{+} ions cm^{-2} is shown in figure 5a. The critical shear stress values range from 15 to 175 MPa with a mean value of 43 MPa. While the mode is in agreement with values from bulk mechanical property tests (Dai and Victoria, 1997), the range suggests that size, position, and orientation of the defect with respect to the dislocation slip plane are important (Hirsch, 1976, Khraishi *et al.*, 2002).

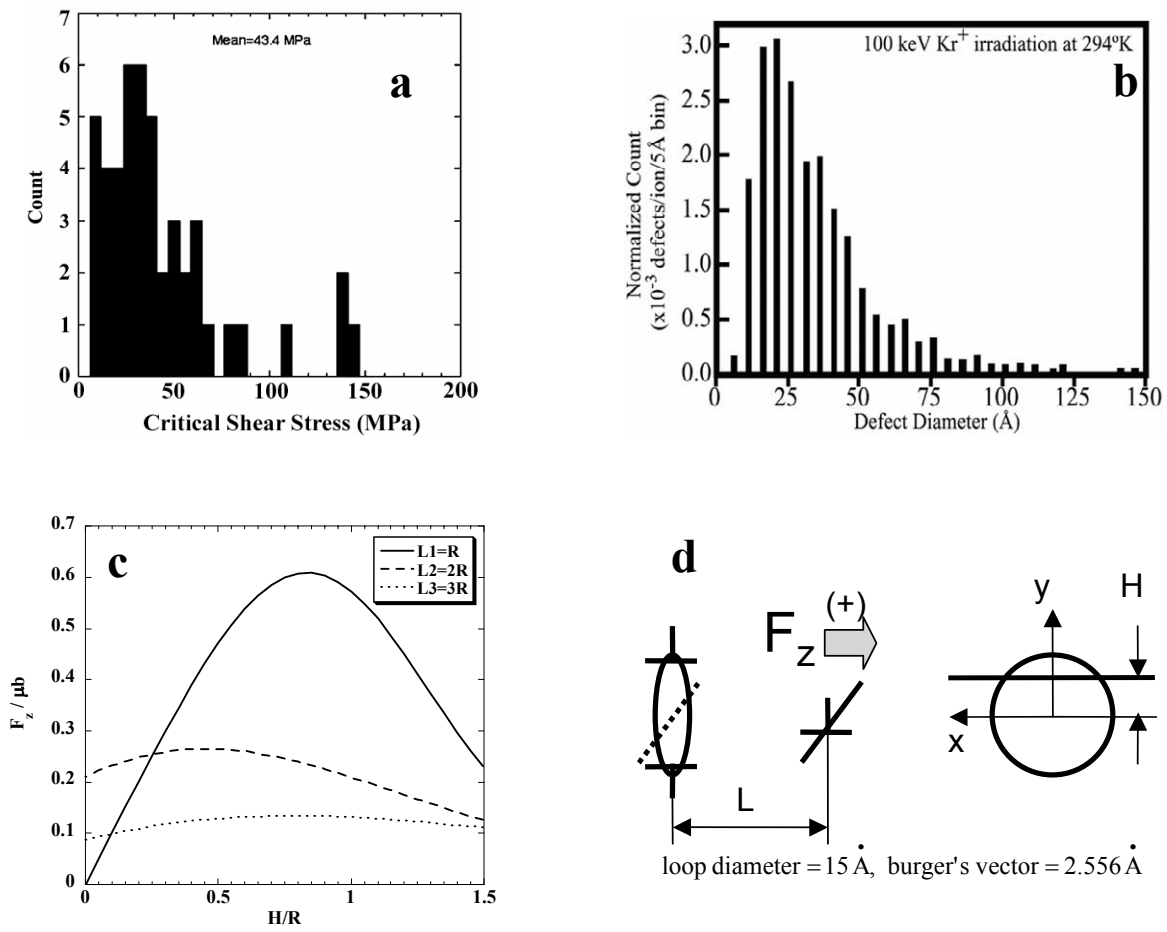

Figure 5. (a) Histogram of the critical shear stress required for breakaway for 51 different interactions. (b) Histogram of defect sizes in heavy-ion irradiated copper to a fluence of 9.6×10^{10} ions cm^{-2}. (c) Total force on an edge dislocation calculated as a function of height, H, and distance from the loop, L. (d) Definition of the variables used in the calculation.

Figure 5b shows a typical size distribution for defects created by a heavy ion irradiation with 100keV Kr^+ ions at room temperature to a dose of 9.6×10^{10} ions cm^{-2} (Daulton *et al.*, 2000). The defect diameters range from 1.5-150 nm. Continuum elasticity calculations based on the integrated Peach-Koehler force between a dislocation and a loop as a function of position were performed. The results are presented in figure 5c, and show a range of interaction forces depending on the height at which the dislocation encounters the loop and the distance at which the dislocation lies. The definitions of the variables in the calculation are depicted in figure 5d.

The combination of defect size distribution and interaction geometry can account for the observed distribution of the pinning strength of the defects.

In the rapidly quenched copper, Frank loops and stacking fault tetrahedra were observed to impede the motion of dislocations during straining. Defect free channels were observed to form in the same manner as in the irradiated specimens. Stacking-fault tetrahedra were also strong barriers to dislocation motion and the interaction resulted in the tetrahedra being annihilated, sheared, or converted to one or more defects (loops and truncated stacking-fault tetrahedra). The details of the interaction could not be discerned experimentally because of the small defect size. To understand the interaction between a dislocation and a stacking fault tetrahedron, molecular dynamics simulations were performed. Specifically, the interaction between dissociated edge dislocations and 2-3 nm stacking fault tetrahedra and overlapping truncated stacking fault tetrahedra in copper were simulated (Diaz de la Rubia *et al.*, 2000, Wirth *et al.*, 2002). In agreement with the dynamic experiments, the simulations show stacking-fault tetrahedra are strong obstacles, they can be sheared by the interaction, and multiple interactions may be required to annihilate the defect. The results of the simulations show that stacking fault tetrahedra are strong obstacles to the motion of dissociated edge dislocations. SFT are sheared, but not absorbed in each dislocation interaction. In the simulation of the interaction of an edge dislocation with a truncated stacking-fault tetrahedron, vacancies are absorbed by the leading edge partial dislocation, creating superjogs as shown in figure 6a. The trailing partial dislocation then constricts at each superjog and climbs through absorption of the remaining vacancies, depicted in figure 6b. Both partial dislocations ultimately pinch-off, creating a perfect loop which can be clearly seen in figure 6c. Figures 6d-f show a similar interaction experimentally.

Here, a perfect dislocation interacts with an isolated tetrahedron, bows around the defect, and finally breaks free of the defect, leaving a perfect loop behind.

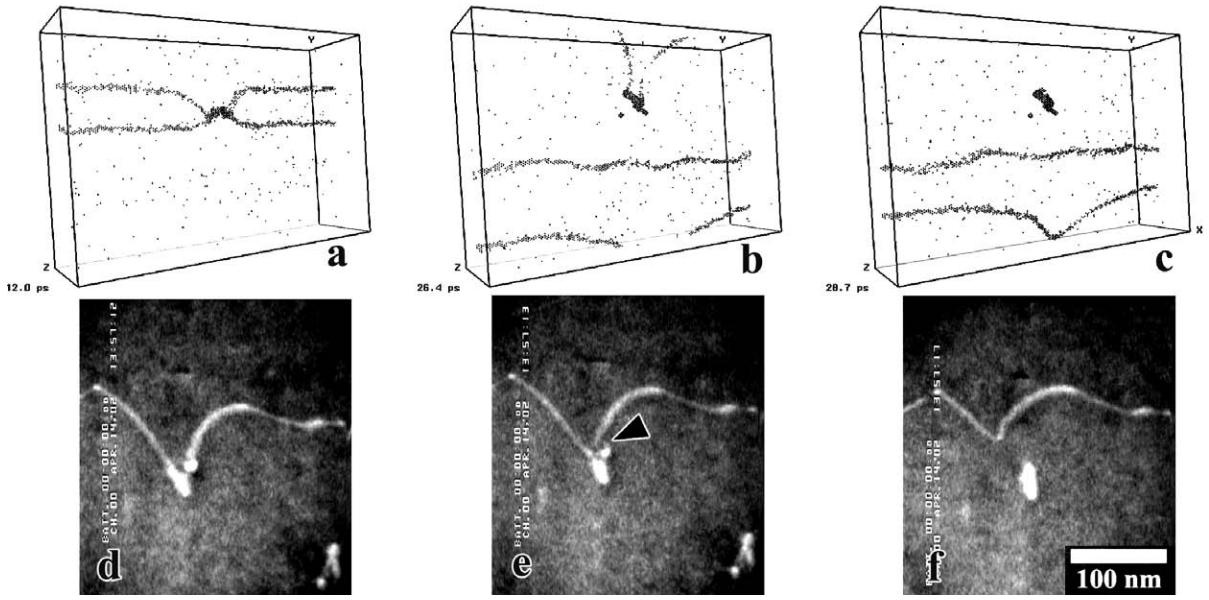

Figure 6. Qualitative comparison of MD simulation (Wirth *et al.*, 2002) and captured WBDF video frames from an *in-situ* TEM straining experiment. (a) The moving dislocation contacts and the partials constrict around the truncated defect. A similar interaction is seen in (d). The leading partial bows around the defect (b) and in the experiment (e), the arrow indicates a newly formed junction. (c) The dislocation has broken away and left behind a perfect loop; the partials have re-entered the simulation cell due to the periodic boundary conditions. (f) The experiment shows the same perfect loop and jogged dislocation resulting from the interaction.

The simulations and dynamic experiments combine to show that the pre-existing dislocations are not responsible for the observed mechanical response. They have also shown that obstacle strength depends on the dislocation character, obstacle type, and geometric effects. In addition, multiple interactions may be required to annihilate a defect, with the nature of the defect being altered during the interactions. These results have been incorporated into a crystal plasticity model of the mechanical response of an irradiated material (Robach *et al.*, 2003). In the model, the total resistance to dislocation motion is defined as the sum of the contributions from dislocations and defects. That is, the total resistance is proportional to $Gb\ (\alpha\rho_{disl} + \beta\rho_{def})^{1/2}$,

where β, is the relative strength of the radiation defects, α the relative strength of the forest dislocations, ρ_{disl} the dislocation density, and ρ_{def} the irradiation-induced defect density.

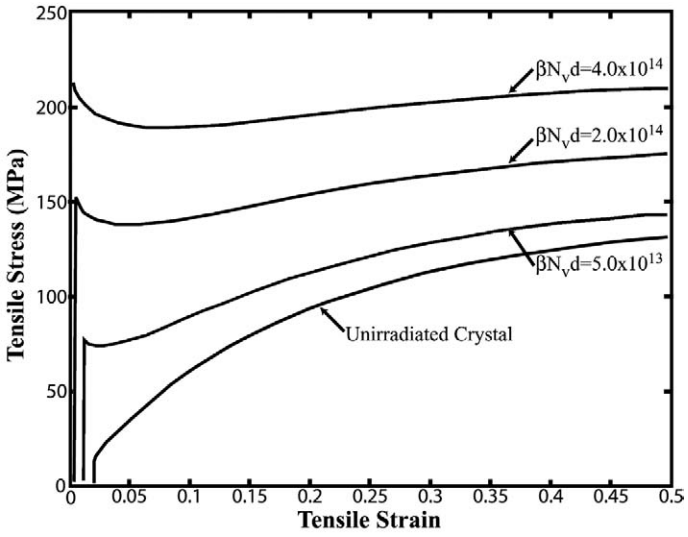

Figure 7. Simulated stress-strain curves for various irradiation-induced defect densities in copper, after (Robach *et al.*, 2003).

In the model, relative obstacle strengths vary with increasing plastic strain as the defects are sheared or altered by the passage of dislocations. The dislocations are allowed to interact with each other within channels and at channel intersections. This is negligible at low strains but becomes significant at high strains. Consequently, the work hardening rate is lower in irradiated than in unirradiated material. At high defect densities the material may work soften due to the fact that the increase in dislocation density is more rapid than the reduction in mobility due to the evolving forest density. The predictions of the model as a function of loop density are shown in figure 7. Qualitatively, these curves are similar to the experimentally measured data, shown in figure 1.

§5. CONCLUSIONS

In-situ straining experiments coupled with molecular dynamics simulations of unit dislocation-defect interactions have provided important observations of the mechanisms that govern defect annihilation and defect-free channel formation. Initial studies have shown:

- The sources of dislocations that create defect-free channels exist in grain boundaries and at local stress concentrations. The pre-existing dislocations do not act as sources but move short distances through the defect fields and are not responsible for the macroscopic mechanical properties.
- The dislocation-defect interaction depends on the character of the dislocation and the type of defect. Multiple interactions may be required to remove the defect.
- The defects are strong barriers to dislocation motion. The barrier strength depends on the dislocation and defect character, and the geometry of the interaction.
- These observations have been used as the foundation for a plasticity model.

ACKNOWLEDGEMENTS

This research was carried out in the DOE National Centre for Microanalysis of Materials in the Frederick Seitz Materials Research Laboratory at the University of Illinois, which is partially supported by the U.S. Department of Energy under grant DEFG02-91-ER45439. Lawrence Livermore National Laboratory supported the work by D. C. Ahn and P. Sofronis under grant DOE LLNL B515082. The work by J. S. Robach and I. M. Robertson was supported by a grant from Lawrence Livermore National Laboratory. The work at LLNL was performed under the auspices of the U.S. Department of Energy by the University of California, Lawrence Livermore National Laboratory under Contract No. W-7405-Eng-48.

REFERENCES

Allen, C. W. and Ryan, E. A., 1997, *Microstructure Evolution During Irradiation*, Materials Research Society Symposium Proceedings, Vol. 439, edited by de la Rubia, T. D. (Warrendale, Pennsylvania: Materials Research Society), pp. 277-87

Dai, Y. and Victoria, M., 1997, *Microstructure Evolution During Irradiation*, Materials Research Society Symposium Proceedings, Vol. 439, edited by Robertson, I. M., Was, G. S., Hobbs, L. W. and Diaz de la Rubia, T. (Warrendale, Pennsylvania: Materials Research Society), pp. 319-324

Daulton, T. L., Kirk, M. A. and Rehn, L. E., 2000, *Phil. Mag. A,* **80,** 809-42.

Diaz de la Rubia, T., Zbib, H. M., Khraishi, T. A., Wirth, B. D., Victoria, M. and Caturla, M. J., 2000, *Nature,* **406,** 871-4.

Fleischer, R. L., 1963, *Acta Metall.,* **11,** 203.
Foreman, A. J. E. and Sharp, J. V., 1969, *Phil. Mag.,* **19,** 931-937.
Friedel, J., 1964, *Dislocations,* (Oxford: Pergamon Press). p. xxi, 491.
Ghoniem, N. M., Tong, S. H., Singh, B. N. and Sun, L. Z., 2001, *Phil. Mag. A,* **81,** 2743-64.
Himbeault, D. D., Chow, C. K. and Puls, M. P., 1994, *Metall. & Mater. Trans. A,* **25A,** 135-45.
Hirsch, P. B., 1976, *Point defect behaviour and diffusional processes*, edited by Harris, J. E. (The Royal Fort, University of Bristol: The Metals Society), pp. 95-107
Khraishi, T. A., Zbib, H. M., De La Rubia, T. D. and Victoria, M., 2002, *Metall. & Mater. Trans. B,* **33B,** 285-96.
Kimura, H. and Maddin, R., 1965, *Lattice defects in quenched metals; an international conference held at the Argonne National Laboratory, June 15-17, 1964, sponsored by the United States Atomic Energy Commission*, edited by Cotterill, R. (New York: Academic Press), pp. 319-386.
Kirk, M. A., Jenkins, M. L. and Fukushima, H., 2000, *J. Nucl. Mater.,* **276,** 50-8.
Kojima, S., Satoh, Y., Taoka, H., Ishida, I., Yoshiie, T. and Kiritani, M., 1989, *Phil. Mag. A,* **59,** 519-32.
Meyers, M. A. and Chawla, K. K., 1984, *Mechanical Metallurgy: Principles and Applications,* (Englewood Cliffs, NJ: Prentice Hall, Inc.).
Muller, G. V., Gavillet, D., Victoria, M. and Martin, J. L., 1994, *J. Nucl. Mater.,* **212-215,** 1283.
Okada, A., Kanao, K., Yoshiie, T. and Kojima, S., 1989, *Mater. Trans. JIM,* **30,** 265-72.
Robach, J. S., Robertson, I. M., Wirth, B. D. and Arsenlis, A., 2003, *Phil. Mag. A***,** Accepted for publication, Nov. 14, 2002.
Saada, G. and Washburn, J., 1963, *Supp. J. Phys. Soc. Jap.,* **18,** 43.
Saka, H., Noda, K., Matsumoto, K. and Imura, T., 1975, *Phys. Stat. Sol. A,* **31,** 139-49.
Singh, B. N., Foreman, A. J. E. and Trinkaus, H., 1997, *J. Nucl. Mater.,* **249,** 103-15.
Singh, B. N., Horsewell, A., Toft, P. and Edwards, D. J., 1995, *J. Nucl. Mater.,* **224,** 131-40.
Stathopoulos, A. Y., 1981, *Phil. Mag. A,* **44,** 285-308.
Sun, L. Z., Ghoniem N.M., Tong, S. H. and Singh, B. N., 2000, *J. Nucl. Mater.,* **283-287 pt.B,** 741-5.
Trinkaus, H., Singh, B. N. and Foreman, A. J. E., 1997, *J. Nucl. Mater.,* **251,** 172-87.
Victoria, M., Baluc, N., Bailat, C., Dai, Y., Luppo, M. I., Schaublin, R. and Singh, B. N., 2000, *J. Nucl. Mater.,* **276,** 114-122.
Wirth, B. D., Bulatov, V. V. and Diaz de la Rubia, T., 2002, *J. Eng. Mater. & Tech. Trans ASME,* **124,** 329-34.
Ziegler, J. F., 1999, *J. App. Phys.,* **85,** 1249-72.